

ORIGINAL RESEARCH

Open Access



Phosphorus-enriched biochar from biogas residue of *Eichhornia crassipes*: transformation and release of phosphorus

Fan Yu^{1,2}, Junxia Wang², Xutong Wang³, Yuting Wang², Qianqian Guo¹, Zhi Wang², Xiaoqiang Cui^{2*}, Yanjun Hu^{1*}, Beibei Yan² and Guanyi Chen^{2,4}

Abstract

Pyrolysis is an effective technology for treating and utilizing biogas residue. To explore the phosphorus (P) supply capacity of the biochar generated from biogas residue of *Eichhornia Crassipes*, the P speciation of *E. crassipes* biogas residue and biomass during pyrolysis (300–700 °C) was analyzed by combining sequential chemical extraction, ³¹P nuclear magnetic resonance (NMR) and P K-edge X-ray absorption near edge structure (XANES) spectroscopy. Pyrolysis treatment promoted the conversion of amorphous Ca-P phases in biogas residue and biomass into crystalline hydroxyapatite (HAP) phase, which matched the formation of stable HCl-P pools in the biochar derived from biogas residue (AEBs, 22.65–82.04%) and biomass (EBs, 13.08–33.52%) in the process of pyrolysis. Moreover, the total P contents in AEBs (19.43–28.92 mg g⁻¹) were higher than that of EBs (3.41–5.26 mg g⁻¹), indicating that AEBs had a great P reclamation potential. The P release kinetics from AEBs and EBs in water were evaluated via an incubation experiment for 360 h. The P release from both AEBs and EBs conformed to the pseudo-second order kinetics model ($R^2 > 0.93$), but their P release behaviors were different. The P release of AEBs conformed to the diffusion-re-adsorption model, while that of EBs accorded with the diffusion-dissolution model. The diffusive gradients in thin-films (DGT) analysis showed that AEBs could significantly increase soil available P content as compared with EBs. Hence, the biochar produced from biogas residue of *E. crassipes* via pyrolysis has a good application potential as a P fertilizer.

Highlights

- Pyrolysis promoted the conversion of amorphous Ca-P phases in biogas residue into crystalline HAP phase.
- The pseudo-second order kinetic model well fitted the experimental data of phosphorus release.
- Biogas residue-derived biochar greatly increased available P content in the soil based on the DGT test.

Keywords Pyrolysis, Phosphorus speciation, Biochar, Release kinetics, Availability

Handling editor: by Xiangzhou Yuan.

*Correspondence:

Xiaoqiang Cui

cuixiaoqiang@tju.edu.cn

Yanjun Hu

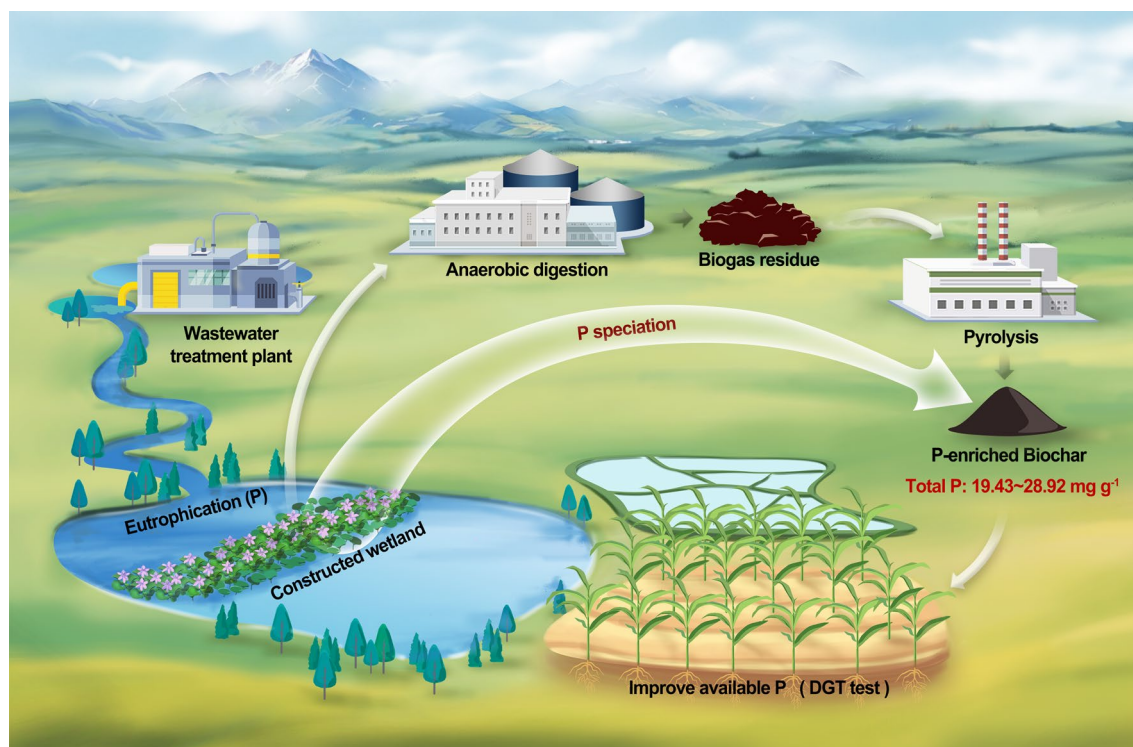
huyanjun@zjut.edu.cn

Full list of author information is available at the end of the article



© The Author(s) 2023. **Open Access** This article is licensed under a Creative Commons Attribution 4.0 International License, which permits use, sharing, adaptation, distribution and reproduction in any medium or format, as long as you give appropriate credit to the original author(s) and the source, provide a link to the Creative Commons licence, and indicate if changes were made. The images or other third party material in this article are included in the article's Creative Commons licence, unless indicated otherwise in a credit line to the material. If material is not included in the article's Creative Commons licence and your intended use is not permitted by statutory regulation or exceeds the permitted use, you will need to obtain permission directly from the copyright holder. To view a copy of this licence, visit <http://creativecommons.org/licenses/by/4.0/>.

Graphical Abstract



1 Introduction

Water eutrophication is posing threats to the water resources worldwide. Constructed wetland, as an efficient, low-cost, and environmentally-friendly technology, is widely used for the removal of nutrient elements from water bodies. As an important part of constructed wetlands, aquatic plants play an important role in the purification of eutrophic water. *Eichhornia crassipes* (water hyacinth) is a ubiquitous aquatic plant in the world. It is extensively employed to treat and purify various eutrophic water bodies, industrial wastewater, and domestic sewage due to its rapid reproduction rate, strong environmental tolerance, and high nutrient absorption rate (e.g., nitrogen, phosphorus, and potassium) (Fazal et al. 2015; Qin et al. 2016; Rezania et al. 2015; Zhang et al. 2019). Meanwhile, *E. crassipes* is also considered a potential raw material for energy production because of its high biomass yield (60–150 tons per hectare) and rich lignocellulose content (about 71.5%) (Guna et al. 2017; Li et al. 2021; Sindhu et al. 2017). The proper C:N ratio (20:1–30:1) and low lignin content (~3.5%) of *E. crassipes* biomass are suitable for microbial decomposition due to the merit of regulating nutrient balance in the anaerobic digestion (AD) process (Feng

et al. 2017; Sindhu et al. 2017). Moreover, compared to other technologies such as composting, pyrolysis, and gasification, AD treatment is simple to operate and can directly dispose of raw materials with high water content. Hence, the most widespread energy research on *E. crassipes* is the production of biogas via AD (Feng et al. 2017). However, the sustainable production of biogas relies on the treatment and proper utilization of biogas residue.

Biogas residue, a by-product of AD, is usually used directly as a fertilizer or soil amendment in agriculture because it contains a high content of nutrients (e.g., phosphorus and nitrogen) for crop growth (Möller and Müller 2012; Tampio et al. 2016). Nonetheless, this disposal method is currently controversial due to its negative impact on the environment, such as emissions of pathogens, odors, organic pollutants, and heavy metals (Insam et al. 2015; Nkoa 2013). Duan et al. (2012) found that the concentrations of As, Cd, Cu, and Zn in paddy soil increased by 2.6, 2.3, 3.2, and 1.8 times, respectively, after being applied the biogas residue from pig manure for one year. This also resulted in the accumulation of As, Cd, Cu, and Zn in cultivated rice plants increased by 1.9, 3.8, 2.2, and 5 times, endangering food security. Moreover, long-term storage and long-distance transportation

will also reduce the economy of biogas residue in agricultural applications because of the limitation of the crop growth stage (Monlau et al. 2015b). In recent years, the conversion of biogas residue into biochar by pyrolysis has attracted extensive attention owing to its environmental and economic benefits, such as the elimination of pathogens, the fixation of organic pollutants and heavy metals, the enrichment of nutrients, and the production of valuable fuels (syngas and bio-oil) (Catenacci et al. 2022; Monlau et al. 2015b, 2016). Compared with biogas residue, the derived biochar has a lower heavy metal toxicity, more stable carbon structure, and higher nutrient content (Hung et al. 2017; Monlau et al. 2016), which is more beneficial to land applications. Ma et al. (2018) and Hung et al. (2017) indicated that biochars produced from biogas residue of dairy and swine manure could be effectively applied to soil as biofertilizers. Opatokun et al. (2017) found that biochar derived from pyrolysis of food waste digestate had low phytotoxicity and promoted tomato seed germination (106–168%) when applied to the soil. Nevertheless, phosphorus (P), as an essential element for plant growth, has rarely been reported in the agricultural application of biogas residue-derived biochar.

Biochar has been proved to be applied to soil as a potential P source, and it can promote plant growth by increasing the availability of P in soil (Gao et al. 2019; Li et al. 2020b; Yang et al. 2021). However, the supply capacity of biochar to soil phosphorus is related to the content and form of P in biochar, which mainly depends on the type of raw materials and pyrolysis conditions (e.g., heating rate, temperature, and residence time) (Adhikari et al. 2019; Chen et al. 2022; Yang et al. 2021). Generally speaking, the P content in biochar derived from sewage sludge (25.2–49.2 mg g⁻¹) and manure (12.5–77.0 mg g⁻¹) is much higher than that from agricultural wastes (1.6–11.6 mg g⁻¹) (Yang et al. 2021). Compared with other pyrolysis parameters, temperature plays a decisive role in the P speciation in biochar, as the transformation of P-containing compounds is highly dependent on pyrolysis temperature (Adhikari et al. 2019). A higher pyrolysis temperature could reduce the availability of P in biochar due to the conversion of labile P to stable P pool (Xu et al. 2016). Although some studies have explored the speciation of P in biogas residue during AD (Li et al. 2020a; Möller and Müller 2012; Tuszynska et al. 2021), the specific form of P in biogas residue-derived biochar is not clear. In addition, the release characteristics of P from biochar will affect the availability and mobility of P, which in turn affect soil P supply, water quality, and overall nutrient management (Liang et al. 2014; Yang et al. 2021). Understanding the P release behavior of biochar can optimize the P supply capacity of soil and minimize

the risk of P leaching loss. Considering that P is predominantly deposited in biogas residue during AD (Möller and Müller 2012; Tuszynska et al. 2021) and will be concentrated into biochar during pyrolysis (Cui et al. 2019; Xu et al. 2016), the biochar prepared from biogas residue of *E. crassipes* has the potential to be applied to soil as a P supplement. Hence, it is necessary to systematically analyze the transformation and release of P in biogas residue-derived biochar from *E. crassipes*.

In this study, biochars were produced from biogas residue and biomass of *E. crassipes* by pyrolysis at different temperatures (300–700 °C). The main purposes of this work were to (1) investigate the transformation of P speciation during pyrolysis of biogas residue and biomass using sequential chemical extraction, ³¹P NMR, and P K-edge XANES spectroscopy, (2) explore the release behavior and mechanism of P from biochar in water, and (3) analyze the P availability of biochar in the soil by employing the diffusive gradients in the thin-film (DGT) technique.

2 Materials and methods

2.1 Biochar preparation and characterization

E. crassipes (EC) was obtained from a constructed wetland in Tianjin, China. The harvested EC was air-dried for a week, and dried in an oven at 80 °C for 24 h. Dry EC (220 g), inoculum, and water were mixed in a 5 L anaerobic digester at a solid–liquid–liquid ratio of 1:10:10, and then put into a 37 °C thermostatic water tank for anaerobic digestion. The biogas residue of *E. crassipes* (AEC) was collected from the anaerobic digester after the anaerobic digestion of dry biomass. The detailed AD process was described in the Additional file 1: Text S1. Biogas residue and biomass were crushed into powder (<0.2 mm) before pyrolysis. The powdered sample in a quartz boat was placed into the center of the horizontal tubular furnace (SKGL-1200C, Jvjing), then heated to the target temperature (300, 500, and 700 °C) under N₂ atmosphere at a heating rate of 10 °C min⁻¹ and held for 2 h. After cooling to room temperature, the biochar was collected and weighed. Biochars derived from AEC and EC were referred to as AEBs and EBs, respectively. In addition, the biochar produced at the target temperature was named as feedstock abbreviation-pyrolysis temperature, e.g., biochar produced from AEC/EC at 500 °C (AEB500/EB500).

Based on the IBI Biochar Testing Guidelines, the ash content of biochar was measured by heating in a Muffle furnace under 750 °C for 5 h, and pH was determined using a pH meter (PHS-3 C, Lei-ci) with a fixed mass/volume ratio of 1:20 for biochar to deionized water. The mineral composition of biochar was analyzed by an X'Pert Pro diffractometer (D/MAX-2500, XRD) at

40 kV and 40 mA over the range of 5–70° with Cu-K α radiation.

2.2 P K-edge XANES analysis

This work was carried out with the support of 4B7A beamline at Beijing Synchrotron Radiation Facility. Our previous studies had shown that aquatic plants such as *Canna indica*, *Hydrocotyle verticillate*, and *Pennisetum purpureum* Schum contain organophosphates (monoester-P), soluble orthophosphate, and Ca-P (Cui et al. 2019, 2020). In addition, considering that soluble phosphate would combine with metal cations (e.g. Fe, Al, Mg) and precipitate into biogas residue in the process of AD (Möller and Müller 2012), the following compounds were selected as reference compounds: phytic acid (sodium salt, PhyAC), K₂HPO₄, K₃PO₄, FePO₄, AlPO₄, MgHPO₄, CaHPO₄, Ca(H₂PO₄)₂, Ca₃(PO₄)₂, hydroxyapatite (Ca₅(PO₄)₃OH, HAP) and octacalcium phosphate (Ca₈H₂PO₄·6.5H₂O, OCP).

Brush phosphorous standards and biochar samples (both in powder form) were evenly on the conductive adhesive, and then remove the excess powder to obtain a uniform film. The XANES data were obtained in fluorescence mode using a silicon drift detector. XANES spectra were collected at 2140–2200 eV. The Athena software was used to analyze XANES data (Ravel and Newville 2005). All spectra were normalized after energy calibration. Linear combination fitting (LCF) of XANES spectra was performed in the range of –12 to +48 eV relative to the edge energy (E₀ = 2151.8 eV). All combinations of reference compounds were used to match each sample. To more accurately detect P species in biochar samples, reference spectra with negative or zero fitting weight were eliminated one by one after the initial fitting, and then repeated the fitting until all reference spectra were positive (Borges et al. 2022). Finally, the combination with the lowest R-factor was selected.

2.3 ³¹P NMR spectroscopy

The ³¹P NMR spectroscopy was used to analyze P speciation in biochar, and detailed operations had been described in our previous study (Cui et al. 2019). In short, P was extracted from the samples by a mixture of 0.25 M NaOH and 0.05 M EDTA, and the freeze-dried extract supernatant was redissolved in D₂O and 1 M NaOH before ³¹P NMR analysis via 400 NMR spectrometer. The ³¹P NMR spectra of EDTA–NaOH were analyzed by MestReNova software.

2.4 Phosphorus chemical extraction

The P in the samples was extracted using an improved sequential extraction method (Xu et al. 2016). In brief, 0.2 g of the sample was successively extracted by 30 mL of

deionized water, 0.5 M NaHCO₃, 0.1 M NaOH, and 1 M HCl solution, and shaken in a incubator at 25 °C for 16 h. The forms of P in each filtered solution after extracting separation were denoted as H₂O-P, NaHCO₃-P, NaOH-P, and HCl-P, respectively. Total phosphorus (P_t) content in biochar and P in sequentially extracted residues (Res-P) were measured by the ascorbic acid method after using H₂O₂–H₂SO₄ digestion. Inorganic P (P_i) in biochar was analyzed after 1 M HCl extraction for 16 h, and organic P (P_o) was calculated by the difference between P_t and P_i. All samples were repeated three times. The P concentration in the solution was determined by the ascorbic acid method (ESS method 310.1) with a UV–Vis spectrophotometer (UV-6000PC, METASH).

2.5 P release from biochar in water

In order to evaluate the P stability of biochar, the release behavior of P from various biochars was determined by batch extraction experiments. The biochar samples (0.1 g) and deionized water were added to a 15 mL centrifuge tubes at a solid–liquid ratio of 1:100, shaken well, and then shocked in a 25 °C constant temperature oscillator at a speed of 150 rpm for 1, 3, 6, 10, 18, 24, 48, 72, 120, 240, and 360 h, respectively. After reaching the target time, the samples were taken out and promptly filtered with a 0.45 μm filter membrane. The concentration of P in the filtrate was measured by the ascorbic acid method. Each sample was repeated three times. The P release kinetics were assessed using five kinetics models (pseudo-first order, pseudo-second order, Elovich, power function, and parabolic diffusion), the equations of which were described in detail by Wu et al. (2021).

2.6 DGT measurement

In comparison with the traditional sequential extraction, the DGT method, as an in-situ sampling technique, can better predict the P availability in soil (Menezes-Blackburn et al. 2016; Ren et al. 2020; Six et al. 2012). The piston-type DGT device was applied in this study to measure the P availability of biochar in the soil. The soil used in the DGT experiment was collected from a farm on the outskirts of Tianjin, China. The pH, P content, and maximum water holding capacity of soil were 7.81, 1.28 mg g⁻¹, and 43%, respectively. 0.3 g biochar and 10 g soil were added to a 100 mL beaker, mixed well, and wetted to 80% of the soil's maximum water-holding capacity. After being incubated in a 25 °C incubator for 2 d, the mixed sample was filled in the lumen of the DGT device, then transferred to a half-open sealed bag containing a small amount of deionized water and incubated again for 2 d. After cleaning the DGT surface with deionized water, the fixed film in the adhesive layer was taken out and extracted in a centrifuge tube containing 10 mL of 1 M NaOH for 2 d. The P concentration

in the extract solution was measured by the ascorbic acid method after removing the fixed film. The P concentration determined by DGT technique (C_{DGT-P}) was calculated according to the following formula:

$$M = \frac{C_e(V_e + V_g)}{f_e} \tag{1}$$

$$C_{DGT} = \frac{M\Delta g}{DA t} \tag{2}$$

where M is the accumulation amount (μg) of the analyte amassed onto the binding layer; C_e is the concentration of the extract; V_e and V_g are the volume of the fixed film and the extraction agent, respectively; f_e is the extraction rate of P on the fixed film; Δg is the thickness of diffusion layer (cm); D is the diffusion coefficient of the target in the diffusion layer ($\text{cm}^2 \text{s}^{-1}$); A is the exposure area (3.14 cm^2); t is the placement time (s) of the DGT device.

2.7 Statistical analysis

The P release kinetics parameters of five different kinetic models were obtained using Origin 2017 software, and the best-fit model was determined by comparing the correlation coefficients (R^2) of different models. SPSS 26.0 software was used for statistical analysis of the data. The correlation between chemical extracted P and DGT-P was determined by the Pearson test at $P < 0.05$.

3 Results and discussion

3.1 Characterization of biochar

The general properties of the biochars derived from biogas residue and biomass of *E. crassipes* are shown in Fig. 1. As the pyrolysis temperature raised, the yield of both AEBs and EBs decreased, while ash content and pH increased (Fig. 1a). This is mainly due to the decomposition of biopolymer (e.g., cellulose, hemicellulose, and lignin) and the accumulation of inorganic components during pyrolysis (Cui et al. 2019). In comparison with

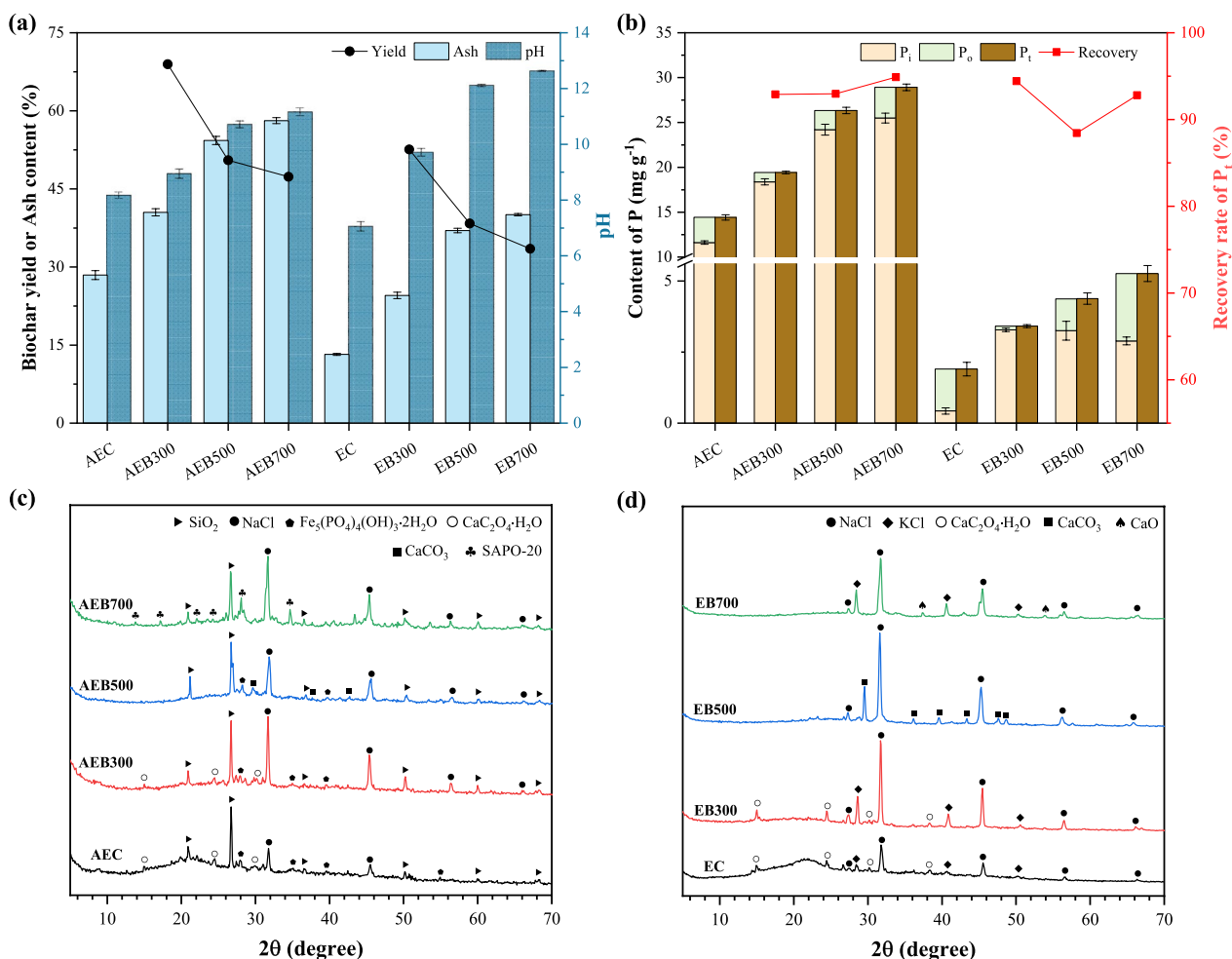


Fig. 1 General properties of the biochars derived from biogas residue (AEBs) and biomass (EBs) of *E. crassipes* at different temperatures. **(a)** Yield, ash content, and pH, **(b)** phosphorus content and recovery rate of P_t, and **(c, d)** X-ray diffraction patterns

EBs, AEBs had higher yields (47.33–68.96%) and ash contents (40.51–58.12%) besides the lower pH (8.94–11.5) at the same temperature. The P_t recovery rate in AEBs and EBs was 92.90–94.89% and 88.43–94.43%, respectively (Fig. 1b), which was consistent with the previous studies (Cui et al. 2019; Huang et al. 2018; Xu et al. 2016), suggesting that the P enrichment degree in the derived biochar from pyrolysis was very high. It is noteworthy that the P_t content in AEBs (19.43–28.92 mg g⁻¹) was one order of magnitude higher than that in EBs (3.41–5.26 mg g⁻¹) and the biochar produced from grass (0.59–4.73 mg g⁻¹) (Yang et al. 2021), pecan shells (0.55–0.22 mg g⁻¹) (Uchimiya et al. 2015), and wheat straw (1.79–3.00 mg g⁻¹) (Xu et al. 2016), implying that the biogas residue-derived biochar had a great P reclamation potential than biomass-derived biochar. Moreover, P_i occupied the dominant position in the biogas residue and AEBs (80.58% and 88.17–94.60%). The biogas residue and AEBs had obvious crystal structures of iron hydroxyl-phosphates ($Fe_5(PO_4)_4(OH)_3 \cdot 2H_2O$) and silicoaluminophosphate-20 (SAPO-20) as compared with biomass and EBs (Fig. 1c, d). This difference might be related to the degradation of organophosphorus and the mineralization of soluble phosphate in biomass during the AD process (Li et al. 2020a; Möller and Müller 2012), which also meant that biogas residue-derived biochar was more conducive to the formation of phosphate mineral crystal phase than biomass-derived biochar.

3.2 P speciation changes during pyrolysis

3.2.1 P K-Edge XANES spectroscopy

Figures 2 and 3 show the LCF of P K-edge XANES spectra and the relative abundance of different phosphates, respectively. The R factors of all samples were lower than 0.008 (Additional file 1: Table S1), which indicated good fitting results. The results of LCF showed that the phosphates in biogas residue were mainly $CaHPO_4$ (46.0%), $Ca(H_2PO_4)_2$ (29.3%), and $FePO_4$ (17.6%), while the phosphates in biomass were mainly $Ca(H_2PO_4)_2$ (68.8%), K_3PO_4 (17.5%) and PhyAC (13.7%). This difference also confirmed that organic phosphate (PhyAC) and soluble phosphate (K_3PO_4) in biomass would be converted into P-containing minerals (mainly Fe-/Ca-P) during AD. Additionally, considering Fe-P and Al-P occupied the dominant position in the phosphate of sludge (Huang and Tang 2016; Shi et al. 2021), the formation of $FePO_4$ and $AlPO_3$ (2.8%) in biogas residue of *E. crassipes* may be partly caused by the residue of fine sludge particles from the inoculant (Additional file 1: Text S1).

The form of P in biogas residue was basically unchanged at 300 °C, but the PhyAC and K_3PO_4 in biomass disappeared completely at the same temperature. Meanwhile, a high proportion of $CaHPO_4$ (68.4%)

occurred in the EB300, which meant that phytate and soluble P in *E. crassipes* biomass would be transformed into amorphous Ca-P at low temperature. Uchimiya et al. (2014, 2015) found that phytates in manure and plant would be transformed into orthophosphate via thermal decomposition during low-temperature pyrolysis (below 350 °C), which was consistent with the transformation of phosphorus form in *E. crassipes* biomass. As the pyrolysis temperature increased from 300 to 700 °C, the relative abundance of $CaHPO_4$ and $Ca(H_2PO_4)_2$ in AEBs decreased from 40.5% and 26.8–14.4% and 0, respectively, while the relative abundance of HAP increased from 0 to 61.7%. Similar changes of Ca-P species were also found in EBs and the derived biochar from animal manures (Huang et al. 2018), suggesting that the amorphous Ca-P phases would transform into crystalline Ca phosphate phases at high temperatures. In addition, compared with EBs, AEBs contained $FePO_4$ (9.3–24.4%) and $MgHPO_4$ (8.3–14.6%) besides Ca-P. The relative abundance of $FePO_4$ in AEBs decreased from 24.4 to 9.3%, which was consistent with the variation trend of Fe-P during sludge pyrolysis (Huang and Tang 2016; Zhu et al. 2022). Zhu et al. (2022) pointed out that the Fe-P in sludge would be converted into Ca-P during pyrolysis due to its reaction with CaO. Notably, no CaO crystals converted from whewellite ($CaC_2O_4 \cdot H_2O$) were found in the XRD pattern of AEBs as compared with EBs (Fig. 1c, d), which indicated that the reaction between $FePO_4$ and CaO also occurred in the pyrolysis process of biogas residue. Moreover, the low abundance of $MgHPO_4$ (4.3%) in biogas residue increased to 8.3% (300 °C), 17.2% (500 °C), and 14.6% (700 °C) during pyrolysis. Considering that struvite would be formed in the process of AD (Wagner and Karthikeyan 2022), this result may be related to the decomposition of struvite during pyrolysis.

3.2.2 Liquid ³¹P NMR spectroscopy

The recovery rates of P_t in biogas residue and biomass of *E. crassipes* extracted by the EDTA-NaOH method were 79.91% and 63.00%, respectively (Additional file 1: Table S3). As the pyrolysis temperature raised, the P_t extraction efficiencies in AEBs and EBs declined, which was consistent with the ³¹P analysis results of pyrolysis-derived biochar from other biological wastes (Cui et al. 2019; Xu et al. 2016). Based on the analysis results of XANES (Fig. 3), the low P_t extraction efficiencies in biochar produced at high temperatures were due to the formation of HAP dissolved only in HCl (Huang and Tang 2016).

The ³¹P NMR spectra (Fig. 4) show that only orthophosphate (ortho-P, ~5.83 ppm) was detected in biogas residue, while monoester-P (~4.28 ppm, 34.36%) was observed in biomass besides ortho-P (65.64%). This

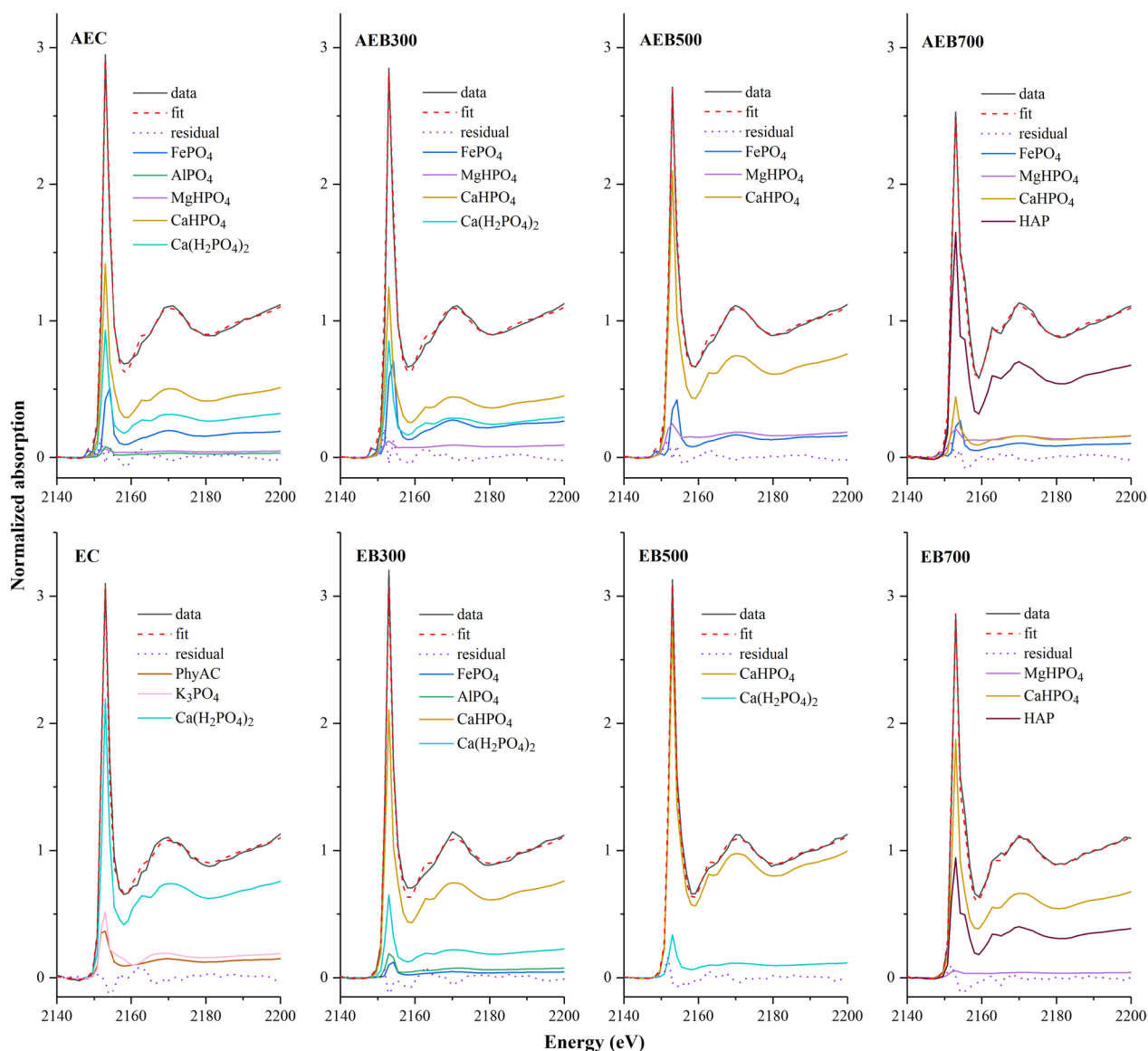


Fig. 2 Linear combination fittings of P XANES spectra of *E. crassipes* biogas residue, biomass, and the derived biochars

result further confirmed that organic P in biomass would degrade in the AD process. The species of P detected in AEBs was the same as that in biogas residue. In comparison with AEBs, pyrophosphate (pyro-P, ~ -4.4 ppm) was observed in the lower temperature derived biochar from biomass (EB300). Uchimiya and Hiradate (2014) pointed out that pyro-P in the low temperature derived biochar was related to polymerization and dehydration of ortho-P, and pyrophosphate would be further converted into orthophosphate at high temperature, which was consistent with the ³¹P NMR spectra results of EBs (Fig. 4b). Moreover, considering that biochar could stabilize pyro-P by hydrogen bonding and bridging cations (Uchimiya

et al. 2015), the absence of pyro-P formation in AEBs might be due to the destruction of surface functional groups in biomass during AD, thus limiting the conversion of ortho-P in biogas residue.

The results of P K-edge XANES and ³¹P NMR analysis basically expounded the P speciation and transformation of biogas residue and biomass during pyrolysis. P in biogas residue was mainly insoluble ortho-P (Fe-/Ca-P) due to the degradation of organic P (PhyAC and monoester-P) and the mineralization and precipitation of soluble ortho-P (K₃PO₄) in biomass during AD. The phosphate in biogas residue was relatively stable at low temperature (300 °C), while PhyAC and monoester-P

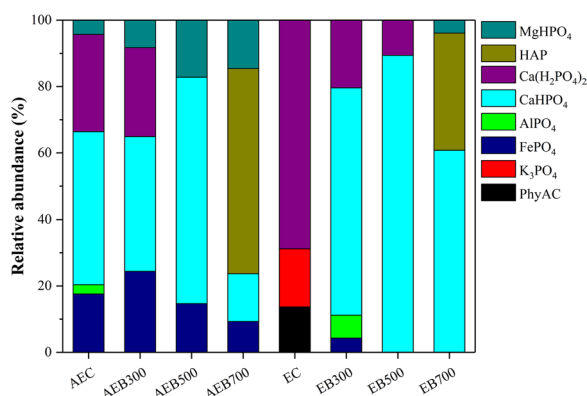


Fig. 3 Relative abundances of different P species in *E. crassipes* biogas residue, biomass, and the derived biochars, as quantified by LCF of their P XANES spectra

in biomass would be decomposed and converted into ortho-P and pyro-P (dehydration). With the increase of pyrolysis temperature, the amorphous Ca-P in biogas residue and biomass would transform into crystalline HAP phase. Compared with EBs, stable Fe-P and Mg-P phases were also observed in AEBs besides Ca-P.

3.3 Sequential extraction of P and its correlation to chemical speciation

Figure 5 and Additional file 1: Table S5 show the distribution and the content of different P pools in *E. crassipes* biogas residue, biomass, and the derived biochars. P in biogas residue was mainly extracted by NaHCO₃ (20.84%), NaOH (47.85%), and HCl (13.24%), but P in biomass was mainly extracted by H₂O (36.59%) and

NaHCO₃ (36.59%). This difference also suggested that water-soluble P and labile-P (NaHCO₃-P) in biomass would be converted into NaOH-P (Fe/Al-associated P) and stable HCl-P pool (e.g., insoluble Ca-P minerals) during AD, which was consistent with the results of XANES analysis. As the pyrolysis temperature raised from 300 to 700 °C, the proportion of NaHCO₃-P and NaOH-P in AEBs declined from 18.70% and 52.17% to 5.09% and 2.38%, respectively, while the HCl-P percentage in AEBs increased from 22.65 to 82.04%. Similar results were found in EBs and the derived biochar from other biowastes (e.g., sewage sludge, wheat straw) (Qian and Jiang 2014; Xu et al. 2016), implying that NaHCO₃-P and NaOH-P would be translated into stable HCl-P pools at high temperature. This result is consistent with the transformation of amorphous Ca-P phases and FePO₄ during pyrolysis and the formation of crystalline Ca phosphate phases (HAP) at high temperature, as revealed in XANES analysis (Fig. 3). Notably, compared with AEBs, EBs had a high fraction of Res-P (38.48–46.23%) in addition to the high HCl-P proportion (33.52–44.07%) at medium/high temperatures (500 and 700 °C). Although the stability of Res-P, as a P pool firmly embedded in mineral and organic structures (Xu et al. 2016; Zhang et al. 2008), was higher than that of HCl-P pool, the higher HCl-P content in the biogas residue-derived biochars at middle/high temperatures (500 and 700 °C) favored the further reclamation of P from biochar via wet chemical techniques (Huang et al. 2017).

In general, the results of sequential extraction were consistent with the P speciation obtained by P K-edge XANES. However, the results of sequential extraction and XANES cannot be completely equated. For example,

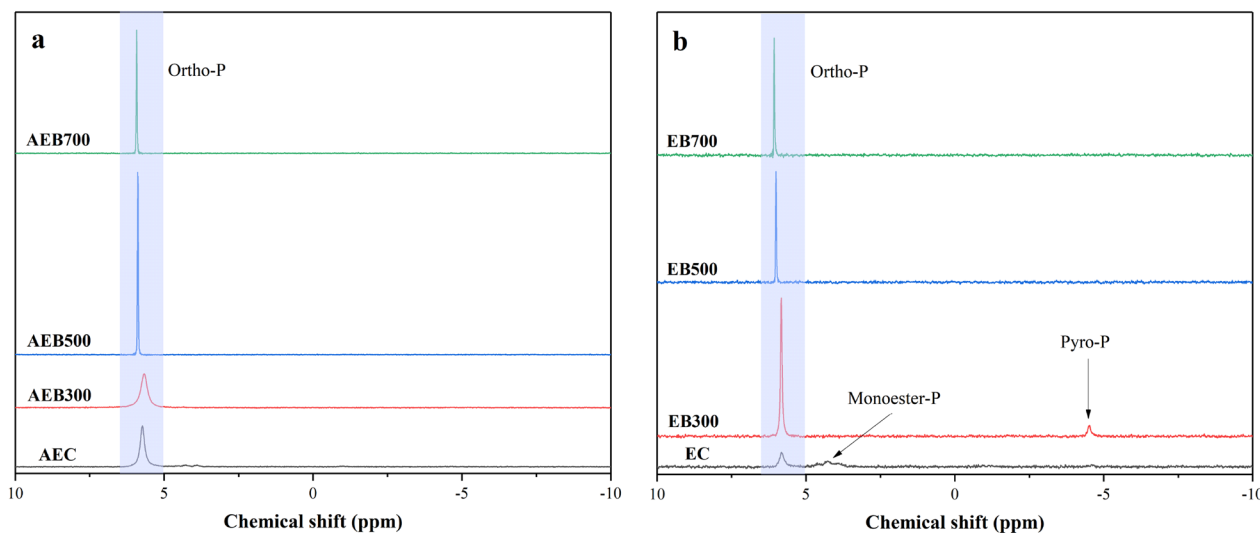


Fig. 4 ³¹P liquid NMR spectra of the biochars derived from (a) biogas residue and (b) biomass of *E. Crassipes*

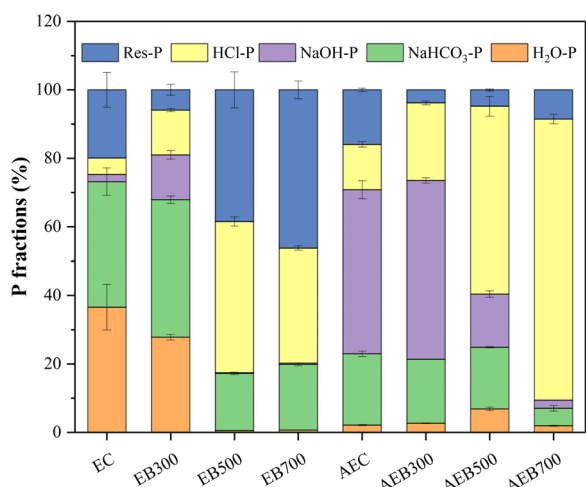


Fig. 5 Distribution of different P pools by sequential extraction of *E. crassipes* biogas residue, biomass, and the derived biochars

the proportion of NaOH-P in biogas residue and AEB300 (47.85% and 52.17%) was much higher than the total relative abundance of Fe-P and Al-P (FePO_4 and AlPO_4) identified by XANES (20.4% and 24.4%). We observed that the biogas residue and AEB300 contained obvious iron hydroxyl-phosphates ($\text{Fe}_5(\text{PO}_4)_4(\text{OH})_3 \cdot 2\text{H}_2\text{O}$) crystals based on XRD analysis (Fig. 1c), but it was not identified in XANES analysis. This result indicated that the absence of reference compounds in XANES analysis could affect the integrity of P species. In addition, P pools from chemical extraction were operationally defined and the P species in each extraction solution are only roughly classified (Huang et al. 2018). Huang et al. explored the correlation between sequential extraction and chemical

morphology of P in sludge and animal manures (Huang et al. 2018; Huang and Tang 2016), and also pointed out that the P species identified by XANES could be qualitatively correlated with the sequentially extracted P forms, but should be cautious in quantitative aspects.

3.4 Release of P in biochars

As depicted in Fig. 6, significant differences were observed on the P release behaviors between biogas residue/AEBs and biomass/EBs. The P release content from biogas residue increased rapidly to 0.23 mg g^{-1} within 10 h, then slowly raised to 0.38 mg g^{-1} within 10–360 h. In comparison with biogas residue, the P release content from biomass reached the maximum (0.70 mg g^{-1}) within 3 h, accounting for 36.86% of its P_t content, which also indicated that AD treatment could reduce the risk of P leaching loss in biomass. For AEBs/EBs, the P release content from the higher temperature derived biochar (AEB700/EB700) was the lowest due to the formation of incompatible crystalline Ca-P phase (Fig. 3). Notably, AEB500 in the biogas residue-derived biochar had the largest P release content, which was consistent with the extraction result of $\text{H}_2\text{O-P}$ in Additional file 1: Table S5. This might be because the P adsorbed on the minerals in biogas residue was released during moderate temperature pyrolysis (Möller and Müller 2012) and refixed at high temperature. In contrast, the P release content of EB300 was the maximum in the biomass-derived biochar due to the transition from soluble-P to stable-P pools. The P release content from AEBs raised rapidly within 18 h and showed a downward trend after 18 h, suggesting that the P released into the water would be re-adsorbed by the biogas residue-derived biochar after a long time. Sun et al. (2018) studied the P dissolution from the

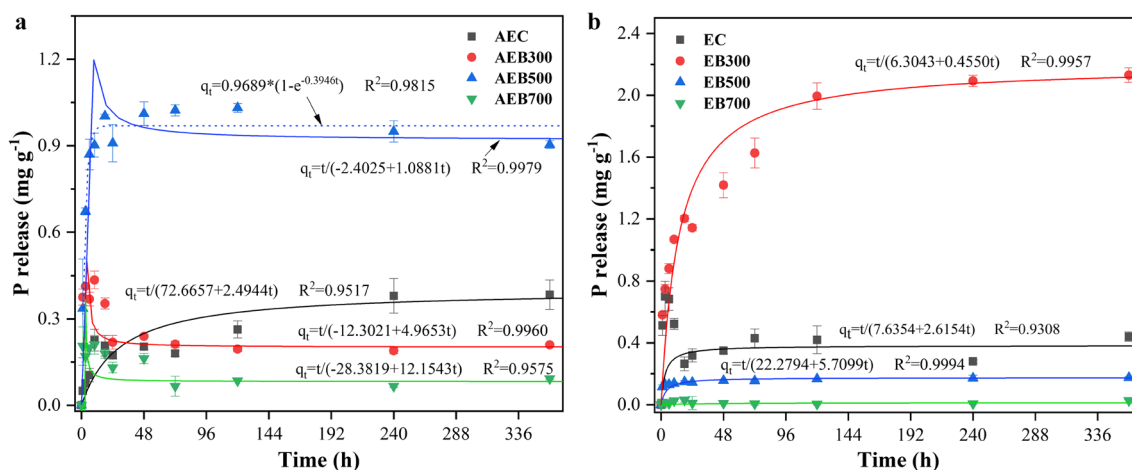


Fig. 6 P release and pseudo-second order kinetics model fitting curves of the biochars derived from (a) biogas residue and (b) biomass of *E. crassipes*

manure- and plant-derived biochar under various water conditions, and also demonstrated that released P into the water could be re-adsorbed on the active sites of biochar surface in the biochar-water system. Compared with AEB300 and AEB700, the decreasing trend of P release in AEB500 was not large after 18 h, which indicated that the moderate temperature derived biochar of biogas residue had a low P adsorption capacity. This might be due to the destruction of the active sites on the AEB500 surface and the underdeveloped pore structure (Sun et al. 2018; Yang et al. 2021). It was noted that the P release content of EBs continued to increase, but the P release rate gradually slowed down with the increase of time, which was very consistent with the P release behavior from manure-derived biochar (Liang et al. 2014), implying that the P release from the biomass-derived biochar conformed to the diffusion-dissolution model.

The P release kinetics parameters and correlation coefficients (R^2) of five different kinetic models are shown in Table 1. Compared with the other four kinetics models, the pseudo-second order kinetics model was more suitable for the kinetics fitting of P release from the derived biochars, and the R^2 of all samples was greater than 0.93 (except EB700). The same fit results were also found in the biochar derived from dairy manure (Liang et al. 2014), rice husks (Qian et al. 2013), switchgrass, and pine tree sawdust (Zhao et al. 2016), indicating that the pseudo-second order kinetic model could well describe the P release behavior from the pyrolysis-derived biochar. In addition, the pseudo-second order kinetic model

implied that the P release from biochar is a chemical process, including external film diffusion, adsorption, and internal particle diffusion (Cui et al. 2022). It is noteworthy that AEBs and EBs had different signs of P release rate constant (k_2), and their fitting curves from pseudo-second order kinetics model (Fig. 6) also had significant differences. The k_2 was greater than 0 in the previous studies of P release kinetics (Liang et al. 2014; Qian et al. 2013), suggesting that P release was a comprehensive process of diffusion and dissolution, which fully accorded with the P release behavior from EBs. Although there was no report that k_2 was less than 0 in the current study, it had been confirmed that biochar could re-absorb the released P into the water via its surface active sites (Sun et al. 2018). Combined with P release behavior from AEBs and fitting curve from pseudo-second order kinetics model, it can be considered that when $k_2 < 0$, P release is a comprehensive process of diffusion and re-adsorption. As for the EB700, all kinetics models did not fit the description of its P release kinetics ($R^2 < 0.47$) due to the extremely low P release content (0.01–0.03 mg g⁻¹). Moreover, the R^2 fitted by the pseudo-first order model to the P release kinetics from AEB500 was 0.9815, indicating that the biogas residue-derived biochar at medium temperature (500 °C) had a very strong P desorption capacity in the short term (Suwanree et al. 2022).

3.5 DGT analysis

The available P can promote the growth and development of plants, and thus increase its yield. Figure 7

Table 1 Correlation coefficients (R^2) and relevant parameters of desorption kinetics models for P release

Equation		Sample							
		AEC	AEB300	AEB500	AEB700	EC	EB300	EB500	EB700
Pseudo-first order $\ln(q_e - q_t) = \ln q_e - k_1 \times t$	R^2	0.7007	0.4568	0.9815	0.3701	0.4569	0.8004	0.9052	0.1272
	k_1	0.0829	233.07	0.3946	62,856	451.33	0.0725	1.311	68,350.27
	q_e	0.2787	0.2919	0.9689	0.1427	0.4476	1.8375	0.1519	0.0132
Pseudo-second order $\frac{t}{q_t} = \frac{1}{k_2 \times q_e^2} + \frac{t}{q_e}$	R^2	0.9517	0.996	0.9979	0.9575	0.9308	0.9957	0.9994	0.4687
	k_2	0.0856	-2.0041	-0.4928	-5.205	0.8959	0.0328	1.4634	1.7993
	q_e	0.4009	0.2014	0.919	0.0823	0.3823	2.1977	0.1751	0.0134
Elovich $q_t = \frac{1}{\beta} \times \ln \alpha \beta + \ln \frac{1}{\beta} \times \ln t$	R^2	0.8287	0.715	0.5628	0.7113	0.3491	0.9562	0.9790	0.0190
	A	0.0303	0.4347	0.6042	0.226	0.6004	0.4191	0.1155	0.0163
	B	0.0538	-0.0442	0.0833	-0.0258	-0.0473	0.2890	0.0101	-0.0007
Power function $q_t = a \times t^b$	R^2	0.8587	0.7408	0.5246	0.6726	0.3064	0.9834	0.9775	0.0785
	a	0.0623	0.4568	0.5554	0.8709	0.5857	0.5904	0.1174	0.0159
	b	0.3182	-0.1538	0.1281	-0.2007	-0.0983	0.2318	0.0693	-0.1015
Parabolic diffusion (PD) $q_t = A + R \times t^{0.5}$	R^2	0.8419	0.6055	0.2172	0.6666	0.2079	0.9048	0.8570	0.0028
	A	0.0828	0.3829	0.7576	0.1986	0.5293	0.7238	0.1269	0.0146
	R	0.0171	-0.0128	0.0163	-0.0078	-0.0115	0.0884	0.0030	-0.0001

Elovich fitting parameter A equal to $1/\beta \times \ln(\alpha\beta)$, B equal to $\ln(1/\beta)$

illustrates the concentration of plant-available P in soil measured by the DGT technique after mixing with *E. crassipes* biogas residue, biomass, and the derived biochars. Compared with the control soil ($103.19 \mu\text{g L}^{-1}$), the DGT-P concentration ($C_{\text{DGT-P}}$) of the mixed samples was significantly improved ($128.08\text{--}480.59 \mu\text{g L}^{-1}$), suggesting that the addition of biogas residue, biomass, and the derived biochars would raise the available P content in soil. This was consistent with the meta-analysis result of available P content in soil with biochar addition (Gao et al. 2019). Li et al. (2016) reported that the application of chemical fertilizers increased the soil available P concentration by 2.1–4.8 times, which was consistent with the effect of biochar addition on soil available P in our study (1.24–4.66 times), implying that the application of biochar could reduce the reliance on chemical fertilizers by improving soil fertility.

The $C_{\text{DGT-P}}$ of the biogas residue-soil mixture ($338.98 \mu\text{g L}^{-1}$) was higher than that of the biomass-soil mixture ($188.34 \mu\text{g L}^{-1}$), implying that AD treatment was beneficial to enhancing the P bioavailability of biomass. Insam et al. (2015) reviewed the fertility of biogas residue from manure, and also found that AD treatment improved the availability of P in manure. The higher DTG-P concentration of the soil-AEBs/EBs mixtures was achieved at lower pyrolysis temperatures, indicating that the low temperature derived biochar would more efficiently improve the P availability in soil. This result was consistent with the trend of potential plant-available P ($\text{NaHCO}_3\text{-P}$ and NaOH-P) content in biochar (Additional file 1: Table S5), so the correlation between DGT-P and $\text{NaHCO}_3\text{-P}/\text{NaOH-P}$ was analyzed. $C_{\text{DTG-P}}$ was highly related with the content of $\text{NaHCO}_3\text{-P}$ ($r=0.936$, $P<0.01$), NaOH-P ($r=0.848$, $P<0.01$), and

$\text{NaHCO}_3\text{-P}+\text{NaOH-P}$ ($r=0.907$, $P<0.01$), indicating that it was reliable to use the $\text{NaHCO}_3\text{-P}$ and NaOH-P to evaluate the P bioavailability in biochar. The good correlation between DGT-P and $\text{NaHCO}_3\text{-P}/\text{NaOH-P}$ ($r=0.57/0.65$, $P<0.01$) was also found in the previous study of soil available P (Menezes-Blackburn et al. 2016), which was consistent with our correlation analysis results. Nevertheless, it was noted that the trend of the correlation coefficients between DGT-P and $\text{NaHCO}_3\text{-P}/\text{NaOH-P}$ were different from the previous study, suggesting that DGT-P in soil with biochar addition cannot be determined simply by the content of $\text{NaHCO}_3\text{-P}$ and NaOH-P in biochar. The P supply ability of biochar to soil depended not only on the content and form of P in biochar, but also on the interaction between biochar and soil, which was affected by soil properties such as pH, cation concentration, phosphatase activity, and microbial community (Gao et al. 2019; Ghodsizad et al. 2021; Jin et al. 2016; Yang et al. 2021). $C_{\text{DTG-P}}$ in the soil added with AEB300/AEB500 ($480.59/462.51 \mu\text{g L}^{-1}$) was significantly higher than that in soil mixed with biogas residue ($338.98 \mu\text{g L}^{-1}$) and EB300/EB500 ($233.53/155.20 \mu\text{g L}^{-1}$), indicating that the biogas residue-derived biochar at low/medium temperatures (300 and 500 °C) had a better potential application as a P fertilizer as compared with biogas residue and the biomass-derived biochar.

4 Conclusions

The reclamation of P from biomass waste has drawn increasing attention due to the shortage of terrestrial P resource worldwide. Converting wetland plant used for eutrophic water purification into biochar and applying it to soil could be a promising scheme to achieve the recovery and reuse of P from eutrophic water. Considering that sequential anaerobic digestion-pyrolysis (AD-pyrolysis) has a higher energy recovery rate and economy feasibility than the single pyrolysis (Monlau et al. 2015a; Wang et al. 2022), the P speciation during pyrolysis of biogas residue from *E. crassipes* was investigated in the present study, which is of great importance to the target application of recovered P. Our results indicated that P in biogas residue was mainly insoluble ortho-P (Ca-/Fe-P), and the amorphous Ca-P in biogas residue would transform into crystalline HAP phase during pyrolysis. In addition, the relative abundance of Fe-P and Mg-P in the biogas residue-derived biochar also changed with the increase of pyrolysis temperature. The DGT results demonstrated that the available P concentration in soil added with the biogas residue-derived biochar was higher than that in soil supplemented with biogas residue, biomass, and the biomass-derived biochar. Therefore, pyrolysis of biogas residue from wetland plant produced alternative P-enriched biochar fertilizers

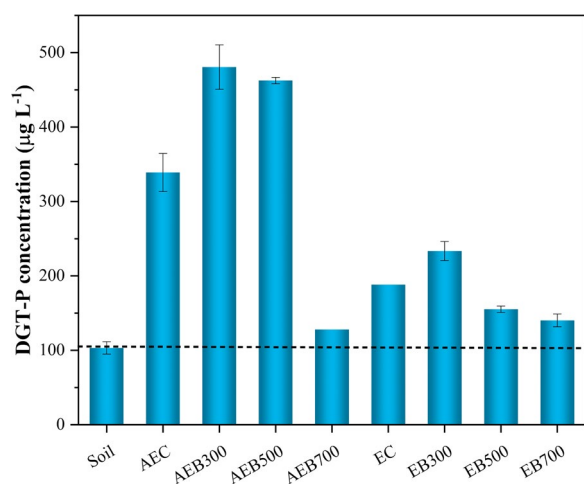


Fig. 7 DGT-P concentration in soil and its mixture with *E. crassipes* biogas residue, biomass, and the derived biochars

with elevated P efficiency as compared with biogas residue, raw wetland plant biomass, and the biomass-derived biochar. Although AD-pyrolysis has a good potential to recover P from *E. crassipes* and achieve the environmentally-friendly utilization of biomass waste, the emission of pollutants and the disposal of biogas slurry during the AD-pyrolysis process should be concerned. Moreover, the cost of storage and transportation from biogas residue and the economic feasibility of AD-pyrolysis scheme should be further evaluated prior to the industrial-scale application. Furthermore, the P transformation in other P-enriched bio-wastes (e.g., animal manure) during AD-pyrolysis can be further explored for optimizing the technical parameters of biochar preparation. Meanwhile, in addition to the species and content of P in the biochar, the P supply ability of biochar to soil was affected by soil properties, phosphatase activity, plant types, microbial community, and climatic conditions. Hence, future studies are also needed to determine the behavior of inherent P in biochar under various agricultural application conditions and optimize the application strategy.

Supplementary Information

The online version contains supplementary material available at <https://doi.org/10.1007/s42773-023-00281-3>.

Additional file 1: Text S1. Anaerobic digestion process of *Eichhornia crassipes*. **Table S1.** R factors and χ^2 of linear combination fitting conducted on P XANES spectra of *E. crassipes* biogas residue, biomass, and the derived biochars at different temperatures. **Table S2.** Relative abundance of different P species determined by LCF fitting of P XANES spectra of *E. crassipes* biogas residue, biomass, and the derived biochars at different temperatures, data were plot in Fig. 3. **Table S3.** Amount of P_i and corresponding recovery rate in *E. crassipes* biogas residue, biomass, and the derived biochars extracted by EDTA-NaOH solution. **Table S4.** Relative abundance of P species in the EDTA-NaOH extracts of *E. crassipes* biogas residue, biomass, and the derived biochars from pyrolysis. Data were calculated from their ³¹P NMR spectra by area integration using NUTS software. **Table S5.** Amount of P (P_i, P_o, P_o) and extracted P by different solutions) in *E. crassipes* biogas residue, biomass, and the derived biochars. **Table S6.** DGT concentration in soil and its mixture with *E. crassipes* biogas residue, biomass, and the derived biochars.

Acknowledgements

The authors thank the Beijing Synchrotron Radiation Facility (4B7A) for the spectra of P K-edge XANES.

Author contribution

FY: Conceptualization, Methodology, Validation, Formal analysis, Writing—original draft. JW: Investigation, Methodology, Software. XW: Validation, Methodology, Investigation. YW: Investigation, Software, Visualization. QG: Data test, Software, Validation. ZW: Conceptualization, Methodology, Validation. XC: Conceptualization, Methodology, Resources, Writing—review and editing, Supervision. YH: Conceptualization, Methodology, Resources, Writing—review and editing, Supervision. BY: Resources, Project administration, Supervision. GC: Resources, Supervision, Funding acquisition. All authors read and approved the final manuscript.

Funding

This study was, in part, supported by a grant from National Natural Science Foundation of China (No. 42107237) and the projects of the key research and development program of Zhejiang Province (No. 2021C03164).

Data availability

The datasets used or analyzed during the current study are available from the corresponding author on reasonable request.

Declarations

Ethics approval and consent to participate

Not applicable.

Consent for publication

The corresponding author consents on behalf of all the authors that this is original work and has permission to be published.

Competing interests

There is no competing interests to declare.

Author details

¹Institute of Energy and Power Engineering, Zhejiang University of Technology, Liuhe Road 288#, Hangzhou 310023, China. ²School of Environmental Science and Engineering, Tianjin Key lab of Biomass Waste Utilization, Tianjin University, Tianjin 300072, China. ³Nuclear and Radiation Safety Center, Ministry of Ecology and Environment, Beijing 100082, China. ⁴School of Mechanical Engineering, Tianjin University of Commerce, Tianjin 300134, China.

Received: 4 August 2023 Revised: 11 November 2023 Accepted: 12 November 2023

Published online: 05 December 2023

References

- Adhikari S, Gascó G, Méndez A, Surapaneni A, Jegatheesan V, Shah K, Paz-Ferreiro J (2019) Influence of pyrolysis parameters on phosphorus fractions of biosolids derived biochar. *Sci Total Environ* 695:133846. <https://doi.org/10.1016/j.scitotenv.2019.133846>
- Borges BMMN, Barreto MSC, Pavinato PS, Teles APB, Strauss M, Abdala DB, Leandro CB, Alves PC, Franco HC (2022) Chemical and spectroscopic evaluations supporting superior P availability after biochar-P fertilizer application. *Soil Tillage Res* 223:105487. <https://doi.org/10.1016/j.still.2022.105487>
- Catenacci A, Boniardi G, Mainardis M, Gievers F, Farru G, Asunis F, Malpei F, Goi D, Cappai G, Canziani R (2022) Processes, applications and legislative framework for carbonized anaerobic digestate: opportunities and bottlenecks. A critical review. *Energy Conv Manag* 263:115691. <https://doi.org/10.1016/j.enconman.2022.115691>
- Chen G, Wang J, Yu F, Wang X, Xiao H, Yan B, Cui X (2022) A review on the production of P-enriched hydro/bio-char from solid waste: Transformation of P and applications of hydro/bio-char. *Chemosphere* 301:134646. <https://doi.org/10.1016/j.chemosphere.2022.134646>
- Cui X, Yang X, Sheng K, He Z, Chen G (2019) Transformation of phosphorus in wetland biomass during pyrolysis and hydrothermal treatment. *ACS Sustain Chem Eng* 7:16520–16528. <https://doi.org/10.1021/acssuschemeng.9b03784>
- Cui X, Lu M, Khan MB, Lai C, Yang X, He Z, Chen G, Yan B (2020) Hydrothermal carbonization of different wetland biomass wastes: phosphorus reclamation and hydrochar production. *Waste Manag* 102:106–113. <https://doi.org/10.1016/j.wasman.2019.10.034>
- Cui H, Dong T, Hu L, Xia R, Zhou J, Zhou J (2022) Adsorption and immobilization of soil lead by two phosphate-based biochars and phosphorus release risk assessment. *Sci Total Environ* 824:153957. <https://doi.org/10.1016/j.scitotenv.2022.153957>
- Duan G, Zhang H, Liu Y, Jia Y, Hu Y, Cheng W (2012) Long-term fertilization with pig-biogas residues results in heavy metal accumulation in paddy field and rice grains in Jiaying of China. *Soil Sci Plant Nutr* 58:637–646. <https://doi.org/10.1080/00380768.2012.726597>
- Fazal S, Zhang B, Mehmood Q (2015) Biological treatment of combined industrial wastewater. *Ecol Eng* 84:551–558. <https://doi.org/10.1016/j.ecoleng.2015.09.014>

- Feng W, Xiao K, Zhou W, Zhu D, Zhou Y, Yuan Y, Xiao N, Wan X, Hua Y, Zhao J (2017) Analysis of utilization technologies for *Eichhornia crassipes* biomass harvested after restoration of wastewater. *Bioresour Technol* 223:287–295. <https://doi.org/10.1016/j.biortech.2016.10.047>
- Gao S, DeLuca TH, Cleveland CC (2019) Biochar additions alter phosphorus and nitrogen availability in agricultural ecosystems: a meta-analysis. *Sci Total Environ* 654:463–472. <https://doi.org/10.1016/j.scitotenv.2018.11.124>
- Ghodsad L, Reyhanitabar A, Maghsoodi MR, Asgari Lajayer B, Chang SX (2021) Biochar affects the fate of phosphorus in soil and water: a critical review. *Chemosphere* 283:131176. <https://doi.org/10.1016/j.chemosphere.2021.131176>
- Guna V, Ilangovan M, Anantha Prasad MG, Reddy N (2017) Water Hyacinth: a unique source for sustainable materials and products. *ACS Sustain Chem Eng* 5:4478–4490. <https://doi.org/10.1021/acssuschemeng.7b00051>
- Huang R, Tang Y (2016) Evolution of phosphorus complexation and mineralogy during (hydro)thermal treatments of activated and anaerobically digested sludge: insights from sequential extraction and P K-edge XANES. *Water Res* 100:439–447. <https://doi.org/10.1016/j.watres.2016.05.029>
- Huang R, Fang C, Lu X, Jiang R, Tang Y (2017) Transformation of phosphorus during (Hydro)thermal treatments of solid biowastes: reaction mechanisms and implications for P reclamation and recycling. *Environ Sci Technol* 51:10284–10298. <https://doi.org/10.1021/acs.est.7b02011>
- Huang R, Fang C, Zhang B, Tang Y (2018) Transformations of phosphorus speciation during (Hydro)thermal treatments of animal manures. *Environ Sci Technol* 52:3016–3026. <https://doi.org/10.1021/acs.est.7b05203>
- Hung C-Y, Tsai W-T, Chen J-W, Lin Y-Q, Chang Y-M (2017) Characterization of biochar prepared from biogas digestate. *Waste Manag* 66:53–60. <https://doi.org/10.1016/j.wasman.2017.04.034>
- Insam H, Gómez-Brandón M, Ascher J (2015) Manure-based biogas fermentation residues—friend or foe of soil fertility? *Soil Biol Biochem* 84:1–14. <https://doi.org/10.1016/j.soilbio.2015.02.006>
- Jin Y, Liang X, He M, Liu Y, Tian G, Shi J (2016) Manure biochar influence upon soil properties, phosphorus distribution and phosphatase activities: a microcosm incubation study. *Chemosphere* 142:128–135. <https://doi.org/10.1016/j.chemosphere.2015.07.015>
- Li WT, Liu M, Jiang CY, Wu M, Chen XF, Ma XY, Li ZP, de Varennes A (2016) Changes in soil aggregate-associated enzyme activities and nutrients under long-term chemical fertilizer applications in a phosphorus-limited paddy soil. *Soil Use Manag* 33:25–33. <https://doi.org/10.1111/sum.12322>
- Li B, Dinkler K, Zhao N, Sobhi M, Merkle W, Liu S, Dong R, Oechsner H, Guo J (2020) Influence of anaerobic digestion on the labile phosphorus in pig, chicken, and dairy manure. *Sci Total Environ* 737:140234. <https://doi.org/10.1016/j.scitotenv.2020.140234>
- Li H, Li Y, Xu Y, Lu X (2020) Biochar phosphorus fertilizer effects on soil phosphorus availability. *Chemosphere* 244:125471. <https://doi.org/10.1016/j.chemosphere.2019.125471>
- Li F, He X, Srishiti A, Song S, Tan HTW, Sweeney DJ, Ghosh S, Wang CH (2021) Water hyacinth for energy and environmental applications: a review. *Bioresour Technol* 327:124809. <https://doi.org/10.1016/j.biortech.2021.124809>
- Liang Y, Cao X, Zhao L, Xu X, Harris W (2014) Phosphorus release from dairy manure, the manure-derived biochar, and their amended soil: effects of phosphorus nature and soil property. *J Environ Qual* 43:1504–1509. <https://doi.org/10.2134/jeq2014.01.0021>
- Ma Q, Song W, Wang R, Zou J, Yang R, Zhang S (2018) Physicochemical properties of biochar derived from anaerobically digested dairy manure. *Waste Manag* 79:729–734. <https://doi.org/10.1016/j.wasman.2018.08.023>
- Menezes-Blackburn D, Zhang H, Stutter M, Giles CD, Darch T, George TS, Shand C, Lumsdon D, Blackwell M, Wearing C, Cooper P, Wendler R, Brown L, Haygarth PM (2016) A holistic approach to understanding the desorption of Phosphorus in Soils. *Environ Sci Technol* 50:3371–3381. <https://doi.org/10.1021/acs.est.5b05395>
- Möller K, Müller T (2012) Effects of anaerobic digestion on digestate nutrient availability and crop growth: a review. *Eng Life Sci* 12:242–257. <https://doi.org/10.1002/elsc.201100085>
- Monlau F, Sambusiti C, Antoniou N, Barakat A, Zabaniotou A (2015) A new concept for enhancing energy recovery from agricultural residues by coupling anaerobic digestion and pyrolysis process. *Appl Energy* 148:32–38. <https://doi.org/10.1016/j.apenergy.2015.03.024>
- Monlau F, Sambusiti C, Ficara E, Aboulkas A, Barakat A, Carrère H (2015) New opportunities for agricultural digestate valorization: current situation and perspectives. *Energy Environ Sci* 8:2600–2621. <https://doi.org/10.1039/c5ee01633a>
- Monlau F, Francavilla M, Sambusiti C, Antoniou N, Solhy A, Libutti A, Zabaniotou A, Barakat A, Monteleone M (2016) Toward a functional integration of anaerobic digestion and pyrolysis for a sustainable resource management. Comparison between solid-digestate and its derived pyrochar as soil amendment. *Appl Energy* 169:652–662. <https://doi.org/10.1016/j.apenergy.2016.02.084>
- Nkoa R (2013) Agricultural benefits and environmental risks of soil fertilization with anaerobic digestates: a review. *Agron Sustain Dev* 34:473–492. <https://doi.org/10.1007/s13593-013-0196-z>
- Opatokun SA, Yousef LF, Strezov V (2017) Agronomic assessment of pyrolysed food waste digestate for sandy soil management. *J Environ Manage* 187:24–30. <https://doi.org/10.1016/j.jenvman.2016.11.030>
- Qian T-T, Jiang H (2014) Migration of phosphorus in sewage Sludge during different thermal treatment processes. *ACS Sustain Chem Eng* 2:1411–1419. <https://doi.org/10.1021/sc400476j>
- Qian T, Zhang X, Hu J, Jiang H (2013) Effects of environmental conditions on the release of phosphorus from biochar. *Chemosphere* 93:2069–2075. <https://doi.org/10.1016/j.chemosphere.2013.07.041>
- Qin H, Zhang Z, Liu M, Liu H, Wang Y, Wen X, Zhang Y, Yan S (2016) Site test of phytoremediation of an open pond contaminated with domestic sewage using water hyacinth and water lettuce. *Ecol Eng* 95:753–762. <https://doi.org/10.1016/j.ecoleng.2016.07.022>
- Ravel B, Newville M (2005) ATHENA, ARTEMIS, HEPHAESTUS: data analysis for X-ray absorption spectroscopy using IFFFIT. *J Synchrotron Radiat* 12:537–541. <https://doi.org/10.1107/S0909049505012719>
- Ren M, Ding S, Shi D, Zhong Z, Cao J, Yang L, Tsang DCW, Wang D, Zhao D, Wang Y (2020) A new DGT technique comprised in a hybrid sensor for the simultaneous measurement of ammonium, nitrate, phosphorus and dissolved oxygen. *Sci Total Environ* 725:138447. <https://doi.org/10.1016/j.scitotenv.2020.138447>
- Rezania S, Ponraj M, Talaiekhosani A, Mohamad SE, Md Din MF, Taib SM, Sabbagh F, Sairan FM (2015) Perspectives of phytoremediation using water hyacinth for removal of heavy metals, organic and inorganic pollutants in wastewater. *J Environ Manage* 163:125–133. <https://doi.org/10.1016/j.jenvman.2015.08.018>
- Shi Y, Chen Z, Cao Y, Fan J, Clark JH, Luo G, Zhang S (2021) Migration and transformation mechanism of phosphorus in waste activated sludge during anaerobic fermentation and hydrothermal conversion. *J Hazard Mater* 403:123649. <https://doi.org/10.1016/j.jhazmat.2020.12.3649>
- Sindhu R, Binod P, Pandey A, Madhavan A, Alphonso JA, Vivek N, Gnansounou E, Castro E, Faraco V (2017) Water hyacinth a potential source for value addition: an overview. *Bioresour Technol* 230:152–162. <https://doi.org/10.1016/j.biortech.2017.01.035>
- Six L, Smolders E, Merckx R (2012) The performance of DGT versus conventional soil phosphorus tests in tropical soils—maize and rice responses to P application. *Plant Soil* 366:49–66. <https://doi.org/10.1007/s11104-012-1375-4>
- Sun K, Qiu M, Han L, Jin J, Wang Z, Pan Z, Xing B (2018) Speciation of phosphorus in plant- and manure-derived biochars and its dissolution under various aqueous conditions. *Sci Total Environ* 634:1300–1307. <https://doi.org/10.1016/j.scitotenv.2018.04.099>
- Suwanree S, Knijnenburg JTN, Kasemsiri P, Kraithong W, Chindaprasit P, Jetsri-suparb K (2022) Engineered biochar from sugarcane leaves with slow phosphorus release kinetics. *Biomass Bioenergy* 156:106304. <https://doi.org/10.1016/j.biombioe.2021.106304>
- Tampio E, Salo T, Rintala J (2016) Agronomic characteristics of five different urban waste digestates. *J Environ Manage* 169:293–302. <https://doi.org/10.1016/j.jenvman.2016.01.001>
- Tuszynska A, Czerwionka K, Obarska-Pempkowiak H (2021) Phosphorus concentration and availability in raw organic waste and post fermentation products. *J Environ Manage* 278:111468. <https://doi.org/10.1016/j.jenvman.2020.111468>
- Uchimiya M, Hiradate S (2014) Pyrolysis temperature-dependent changes in dissolved phosphorus speciation of plant and manure biochars. *J Agric Food Chem* 62:1802–1809. <https://doi.org/10.1021/jf4053385>
- Uchimiya M, Hiradate S, Antal MJ (2015) Dissolved phosphorus speciation of flash carbonization, slow pyrolysis, and fast pyrolysis biochars. *ACS*

- Sustain Chem Eng 3:1642–1649. <https://doi.org/10.1021/acssuschemeng.5b00336>
- Wagner E, Karthikeyan KG (2022) Precipitating phosphorus as struvite from anaerobically-digested dairy manure. *J Clean Prod* 339:130675. <https://doi.org/10.1016/j.jclepro.2022.130675>
- Wang Z, Li J, Yu F, Yan B, Chen G (2022) Comprehensive evaluation of gradient-controlled anaerobic digestion and pyrolysis integration processes: a case study of Sargassum treatment. *Bioresour Technol* 345:126496. <https://doi.org/10.1016/j.biortech.2021.126496>
- Wu W, Yan B, Zhong L, Zhang R, Guo X, Cui X, Lu W, Chen G (2021) Combustion ash addition promotes the production of K-enriched biochar and K release characteristics. *J Clean Prod* 311:127557. <https://doi.org/10.1016/j.jclepro.2021.127557>
- Xu G, Zhang Y, Shao H, Sun J (2016) Pyrolysis temperature affects phosphorus transformation in biochar: chemical fractionation and (31)P NMR analysis. *Sci Total Environ* 569–570:65–72. <https://doi.org/10.1016/j.scitotenv.2016.06.081>
- Yang L, Wu Y, Wang Y, An W, Jin J, Sun K, Wang X (2021) Effects of biochar addition on the abundance, speciation, availability, and leaching loss of soil phosphorus. *Sci Total Environ* 758:143657. <https://doi.org/10.1016/j.scitotenv.2020.143657>
- Zhang R, Wu F, Liu C, Fu P, Li W, Wang L, Liao H, Guo J (2008) Characteristics of organic phosphorus fractions in different trophic sediments of lakes from the middle and lower reaches of Yangtze River region and Southwestern Plateau, China. *Environ Pollut* 152:366–372. <https://doi.org/10.1016/j.envpol.2007.06.024>
- Zhang Y, Liu H, Yan S, Wen X, Qin H, Wang Z, Zhang Z (2019) Phosphorus removal from the hyper-eutrophic Lake Caohai (China) with large-scale water hyacinth cultivation. *Environ Sci Pollut Res Int* 26:12975–12984. <https://doi.org/10.1007/s11356-019-04469-8>
- Zhao L, Cao X, Zheng W, Scott JW, Sharma BK, Chen X (2016) Copyrolysis of Biomass with phosphate fertilizers to improve Biochar Carbon Retention, slow nutrient release, and stabilize Heavy metals in Soil. *ACS Sustain Chem Eng* 4:1630–1636. <https://doi.org/10.1021/acssuschemeng.5b01570>
- Zhu Y, Zhao Q, Li D, Li J, Guo W (2022) Performance comparison of phosphorus recovery from different sludges in sewage treatment plants through pyrolysis. *J Clean Prod* 372:133728. <https://doi.org/10.1016/j.jclepro.2022.133728>

Submit your manuscript to a SpringerOpen[®] journal and benefit from:

- Convenient online submission
- Rigorous peer review
- Open access: articles freely available online
- High visibility within the field
- Retaining the copyright to your article

Submit your next manuscript at ► [springeropen.com](https://www.springeropen.com)
